

TOMASZ NOWICKI\*

THE DISCRETE VORTEX METHOD  
FOR ESTIMATING HOW SURFACE ROUGHNESS  
AFFECTS AERODYNAMIC DRAG ACTING  
ON A LONG CYLINDER EXPOSED TO WIND

OSZACOWANIE WPŁYWU CHROPOWATOŚCI  
POWIERZCHNI NA SIŁĘ OPORU AERODYNAMICZNEGO  
DZIAŁAJĄCEGO NA DŁUGI WALEC  
ZA POMOCĄ METODY WIRÓW DYSKRETNYCH

Abstract

This paper focuses on the aerodynamic drag force that acts on a long cylinder standing up to aerodynamic wind in the critical regime of the fluid flow. The core problem addressed here is how surface roughness of a high level and further increase of that level affects the drag. The research is based on computer simulations using the Discrete Vortex Method. A meshless version of the method was applied in order to let the boundary layer form freely in the way of a direct computer simulation. Fundamental ideas behind the Discrete Vortex Method, the original research program and the obtained results are presented. The main conclusion is that a small level of surface roughness may be neglected in engineering estimations.

*Keywords:* wind engineering, discrete vortex method, surface roughness, aerodynamic force, aerodynamic drag

Streszczenie

W pracy skupiono się na sile oporu aerodynamicznego działającej na nieskończenie długi walec poddany działaniu wiatru w zakresie krytycznym przepływu. Centralnym zagadnieniem badań było określenie wpływu dużej chropowatości walca na wartość tej siły oraz określenie związku pomiędzy zmianą parametru chropowatości a jej wartością. W ramach badań wykonano serię symulacji komputerowych przy użyciu metody wirów dyskretnych. Została zastosowana beziarkowa implementacja metody w celu osiągnięcia efektu swobodnego formowania się warstwy brzegowej. Praca przedstawia podstawy teoretyczne metody wirów dyskretnych, założenia programu badań autorskich oraz uzyskane wyniki. Głównym wnioskiem postawionym w pracy jest określenie poziomu chropowatości poniżej którego może ona być zaniedbana w oszacowaniach inżynierskich.

*Słowa kluczowe:* inżynieria wiatrowa, metoda wirów dyskretnych, chropowatość, opór aerodynamiczny

DOI: 10.4467/2353737XCT.15.129.4166

\* Department of Structural Mechanics, Lublin University of Technology, Poland.

## 1. Introduction

The knowledge of how surfaces roughness affects the aerodynamic response of solid bodies during exposure to wind is very important for a wide spectrum of technical problems. The ability of determining the level below which the roughness may be neglected is very useful from an engineering point of view. The upper limit of surface roughness is similarly very important. The upper limit of surface roughness is defined here as its size that is not yet the change in shape of the original body. The presented paper fits in long lasting interest in flows past circular cylinders. The flows are not only theoretical problems but also are very important from a practical point of view in relation to engineering structures. It is well known that the flow past a circular cylinder can be categorised according to the Reynolds number as subcritical, critical, supercritical or transcritical. In the critical regime ( $Re \approx 1 \cdot 10^5 - 5 \cdot 10^5$ ) the phenomenon combines flow separation, turbulence transition, reattachment and turbulent separation of a boundary layer. The transition causes delaying of the separation point, which results in a reduction of the resultant drag force acting on the cylinder. On the other hand, high level surface roughness of the cylinder strongly effects the turbulent boundary layer making the process much more complicated.

This work aims at finding out how surface roughness changes the resultant aerodynamic drag force (expressed here as a drag force coefficient) under conditions of complex physics. For this purpose, Discrete Vortex Method (DVM) computer simulations were carried out. This method was chosen due to its meshless nature, which lets the turbulence (including boundary layer) form freely in the way of direct computer simulation. The main asset of DVM compared to a mesh-based method (e.g. the finite volume method) is the lack of artificial models of turbulence like RANS, LES or k- $\epsilon$ . Computer simulations were carried out at Reynolds number values of  $0.7 \cdot 10^5$ ,  $1.3 \cdot 10^5$ ,  $2.0 \cdot 10^5$ ,  $2.7 \cdot 10^5$  for 5 different levels of surface roughness. It would not be a surprise that increasing roughness poses a growing challenge due to increases in the complexity of the phenomena to be modelled. Three parameters describing surface roughness have been introduced. Finally, the obtained results allowed determining the levels of surface at which a) it can be neglected in engineering estimations, b) it means a change in the shape of the original object.

## 2. Problem description

The inspiration for the presented research comes from engineering practice. Real objects such as cables, pipes, or circular chimneys are never with a completely smooth surface. It is always a decision for an engineer whether the roughness can or cannot be neglected when the object is studied in a wind tunnel or numerically modelled. This work is intended to be an aid during the decision making process.

The object of study is a circular cylinder (Fig. 1a) long enough in order to treat the air flow around it as a 2D case. The cylinder is subjected to an air stream at speed  $u_{AIR}$ , which results in the appearance of aerodynamic forces:  $F_X$  – drag,  $F_Y$  – lift,  $M$  – moment. This research focuses on the drag force. The cross-section of the cylinder has been designed to be cogwheel

shaped (Figs. 1b, 2b), which simulates surface roughness. Each cogwheel is composed of 18 cogs in the shape of equilateral triangles uniformly distributed around the mean diameter  $D_{\text{MEAN}}=0.2\text{m}$ . The mean diameter, that is also the outline of the cylinder with surface of zero roughness, crosses each of the cogs in the middle of its depth, which is illustrated in Fig. 3. The number of cogs is a compromise between the complexity of the numerical models and the requirement of similarity to real surface roughness and has been found by way of preliminary study. Five levels of roughness have been taken into consideration (Fig. 2). In order to describe the level of roughness, three dimensionless parameters have been introduced. The first one  $f_1$  is a ratio of cavity depth ( $h = 0.000 \text{ m}, 0.005 \text{ m}, 0.010 \text{ m}, 0.020 \text{ m}, 0.030 \text{ m}$ ) to the mean diameter of the cylinder  $D_{\text{MEAN}}$  (Fig. 3):

$$f_1 = h / D_{\text{MEAN}} \quad (1)$$

The parameter does not consider the total volume of cavity in the cylinder surface. On the contrary the second parameter of roughness (Fig. 4):

$$f_2 = A_{\text{CLOSE}} / A_{\text{OUT}} \quad (2)$$

where  $A_{\text{CLOSE}}$  is the total area of the cavity in the cross-section plane,  $A_{\text{OUT}} = \pi D_{\text{OUT}}^2/4$  is the area of the circle enclosing the outline of the cross-section – this does not include any direct information on roughness depth. The parameter  $f_2$  applied to the 3D object refers to volumetric size of the cavity on the surface. The third parameter of roughness (Fig. 5):

$$f_3 = (L_{\text{COG}} - L_{\text{MEAN}}) / L_{\text{MEAN}} \quad (3)$$

where  $L_{\text{MEAN}} = \pi D_{\text{MEAN}}$  is a circumference of the original cylinder while  $L_{\text{COG}}$  indicates the perimeter of the real shape, describe the increment in surface area when applied to 3D object. This indirectly contains information about the size and the amount of surface cavity. For the studied case when the surface roughness is generated as regular geometry, all the parameters are of course geometrically correlated but for real uniformly distributed roughness, the correlation would not be so simple and this is the reason for introducing the parameters independently. Table 1 lists values of the defined parameters of roughness for the cross-sections used in the numerical experiment.

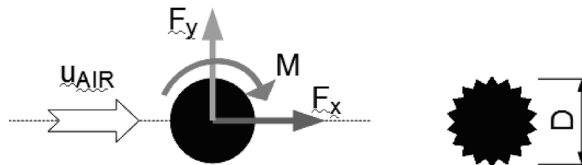


Fig. 1. The object of study: a) circular cylinder in an air stream at speed  $u_{\text{AIR}}$  with resulting aerodynamic forces:  $F_x$  – drag,  $F_y$  – lift,  $M$  – moment; b) structure of surfaces roughness of the cylinder  $D = 0.20 \text{ m}$  – mean diameter

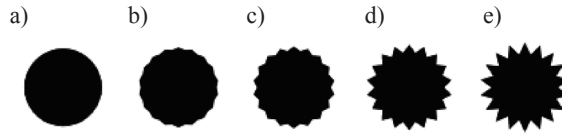


Fig. 2. View of the cross-section of the cylinder under study introduced according to growing roughness of its surface

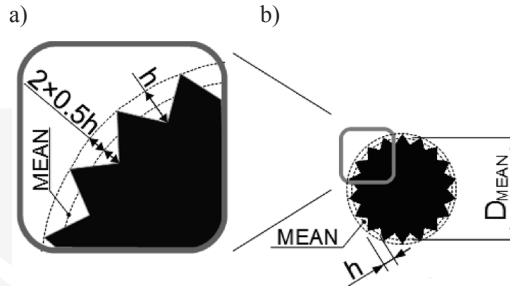


Fig. 3. View of geometrical structure of the roughness being generated on surface of the cylinder under study: a) close-up, b) general view. The uniform cog-wheel shape with depth of  $h$  is evenly distributed about the contour of the original cylinder with diameter  $D_{MEAN}$

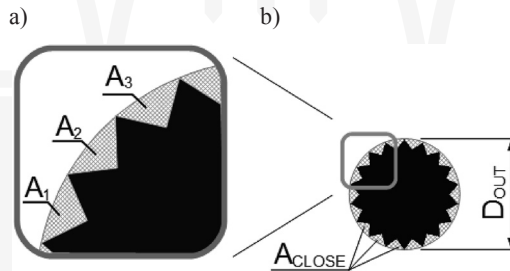


Fig. 4. View of a closing area ( $A_{CLOSE} = A_1 + A_2 + A_3 + \dots$ ) that is needed to smoothed the rough surface of the cylinder: a) close-up, b) general view,  $D_{OUT}$  – diameter of resulting cylinder

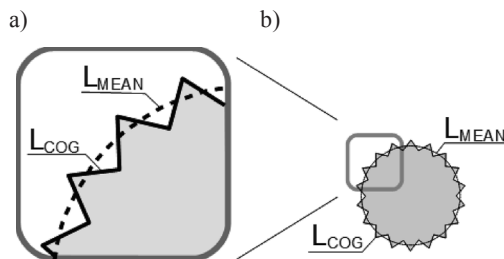







Fig. 5. View of a real perimeter of the cog-wheel shape  $L_{COG}$  compared to circumference of original shape  $L_{MEAN}$ : a) close-up, b) general view

**Values of parameters of roughness for the cross-sections used in the study**

	a) 	b) 	c) 	d) 	e) 
$h$ [m]	0.000	0.005	0.010	0.020	0.030
$f_1$ [%]	0.0	2.5	5.0	10.0	15.0
$f_2$ [%]	0.0	5.3	10.0	18.5	26.5
$f_3$ [%]	0.0	3.9	15.0	51.7	98.2

The consecutive cross-sections of the cylinder simulate growing roughness of its surface. It can be seen clearly that the choice of parameter determines the quantitative description of the roughness. Moreover, it is not the absolute values that is the most important in the description but their increments between the next levels of roughness. This characteristic determines which of them would be the most useful in a specific engineering problem.

### 3. Discrete Vortex Method

#### 3.1. Theoretical background of DVM

Discrete Vortex Method (DVM) is a numerical method developed for solving the Navier–Stokes equation (N-S) based on the Lagrangian model of a particle tracing. In DVM, the equation is solved by the direct computer simulation of a physical phenomena. A finite mesh known from finite element and finite volume methods is not applied in DVM. Artificial models of turbulence such as LES or k- $\epsilon$  are also not used.

Considering 2D areas of fluid flow and assuming a homogeneous dry air with a constant density, the following form of the N–S equation can be used to describe the phenomenon under interest [1]:

$$\frac{\partial \mathbf{u}}{\partial t} + (\mathbf{u} \cdot \nabla) \mathbf{u} = -\frac{1}{\rho} \nabla p + \nu \Delta \mathbf{u} \quad (4)$$

where:  $\mathbf{u}$  – velocity field,  $p$  – pressure field,  $\rho$  – density,  $t$  – time,  $\nu$  – kinematic viscosity. The part  $(\mathbf{u} \cdot \nabla)$  is an operator.

Eq. (5) is decomposed by calculating the rotation of the vector  $\mathbf{u}$ , which gives the so-called vorticity transport equation:

$$\frac{\partial \boldsymbol{\omega}}{\partial t} + (\mathbf{u} \cdot \nabla) \boldsymbol{\omega} = \nu \Delta \boldsymbol{\omega} \quad (5)$$

where  $\boldsymbol{\omega} = \nabla \times \mathbf{u}$  is a vorticity field of the flow. The last equation (5) is composed of two components: advection (6) and diffusion (7):

$$\frac{\partial \boldsymbol{\omega}}{\partial t} + (\mathbf{u} \cdot \nabla) \boldsymbol{\omega} = 0 \quad (6)$$

$$\frac{\partial \boldsymbol{\omega}}{\partial t} = \nu \Delta \boldsymbol{\omega} \quad (7)$$

The separation lets us treat the fluid flow as two simultaneous and independent phenomena – advection and diffusion – and is known as a split algorithm. In DVM, it is not the velocity field that is being directly simulated but its vorticity equivalent. The vorticity field is represented in a discrete form, which for the 2D case reduces to a set of particles to a so-called vortex cloud. Each vortex particle contributes to the total cloud velocity field of flow that it co-represents, under the aerodynamic Bio–Savart law. Assembly of the cloud velocity field and potential velocity field not included in (5) but present in (4) gives the final velocity field in which the vortex cloud is drifted. The process is described by the advection formula (6). While the diffusion (7) is implemented as the vortex cloud erosion caused by the viscosity of the fluid medium.

The source of vorticity in the flow is a solid body immersed in it. Saying precisely the solid-fluid border. Because fluid velocity at the border is zero, there is a need to cover the body with a vortex sheet that reduces the influence of the environment outside the body. The sheet is created and shed at every simulation step. Vortex particles that have been shed become members of the vortex cloud.

The vortex sheet also determines pressure distribution on the solid body. After completing advection and diffusion simulation steps, the N–S Eq. (5) reduces to:

$$\frac{\partial \mathbf{u}}{\partial t} = -\frac{1}{\rho} \nabla p \quad (8)$$

which is the base to find the distributions under interest and finally resulting forces  $F_x$ ,  $F_y$ ,  $M$  acting on the cylinder.

### 3.2. DVM applications in wind engineering

The origin of DVM dates back to the 1930s. However, fast developments in vortex methods started in the 1980s, preceded by the progress in computer technology. Since then, DVM has been successfully applied to many scientific and engineering problems. Many of them have entered the canon of research literature.

The first example [2] concerns a real building included in the Texas Tech University campus. The building was equipped with measuring utilities allowing monitoring parameters of wind flow over it. It was localized in a flat open area far from other buildings. The wind

flow had an angle-of-attack of  $90^\circ$  with respect to the longest wall of the building. In the computer DVM simulations, the problem was simplified to a 2D flow case. The numerical simulation was performed for the Reynolds number  $Re = 2.3 \cdot 10^6$ . Numerical results were compared with experimental data. Selected results are presented in Fig. 6. The example shows good conformity between numerical simulation results and experimental data. The most important achievement is the shape of the line obtained from computer simulations. This shows that DVM algorithms are able to model the phenomena of turbulence that occurs near corners. The discrepancy between the experiment and the calculations comes from the fact that the building was not long enough (the length to depth ratio was equal to 1.5) to treat the flow as two dimensional and the influences of walls parallel to the flow should not have been neglected and three dimensional analysis of the flow would have been more proper in this case. However, the differences are small and do not disqualify the results from a civil engineer's point of view.

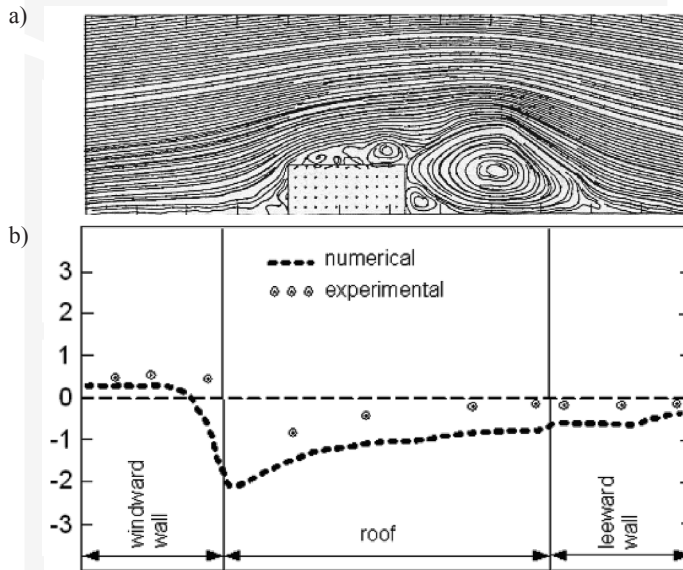


Fig. 6. Wind flow over a Texas Tech building [2]: a) streamlines obtained from computer simulations, b) mean pressure coefficients numerical and experimental

The second problem [3] concerned finding coefficients of aerodynamic resistance: drag, lift and moment, by way of DVM computer simulations. Square and rectangular sections were analyzed against wind action with a different angle of incidence. The shape ratio varied from  $1/4$  to  $3$  and the angle of incidence evolved from  $45$  to  $90$  degrees. Two-dimensional flow was assumed. During the simulations, the Reynolds number came to  $2 \cdot 10^4$ . Numerical results were confronted with experimental data. The conclusion was that DVM analysis may be successfully used for determining aerodynamic coefficients for engineering practice.

Undeniable superiority to other CFD methods DVM presents in analysis including aeroelastic interaction. An example of such a simulation one can find at [4], where the authors

presented their results of the dynamic response of a bridge glider placed in a turbulent wind flow. They used DVM to examine the aero-elastic stability of Tacoma Narrow Bridge and compared the results with historical experimental data. Numerical simulations concerned only the deck of the bridge. Because flutter occurred in the center area of the bridge and the bridge span was a few dozen times longer than its width, simplification to 2D analysis was justified and did not introduce big errors.

Computer calculations reconstructed the catastrophe that happened in 1940. Numerical experiments conducted for wind speed in a range from 5 to 20 m/s. They confirmed that the critical speed for flutter was 19 m/s, which was consistent with historical data.

### 3.3. DVM implementation – in home solver

Computer simulations presented in this paper were carried out using an original computer program Ventus2D developed by the author [5]. The computer program implements algorithms of DVM and, at its present stage of development, it is able to simulate fluid flow around a solid body of random shape by way of direct numerical calculations (Fig. 7). The solid body immersed in fluid can be stationary (i.e. fixed) or elastically suspended (with or without damping). In both cases, a boundary layer phenomenon, turbulence effects (e.g. vortex street) and interaction between a solid body and fluid are effects of ‘intelligent’ DVM algorithms. The DVM solver does not use any mesh. All vortexes are free to move in the calculation domain.

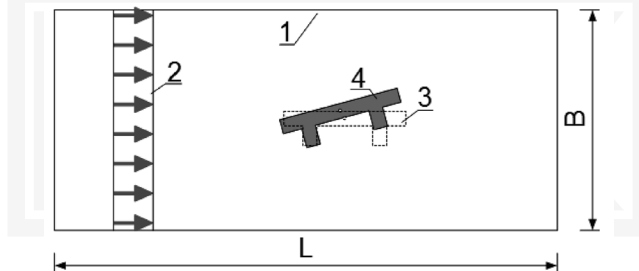


Fig. 7. Diagram of an aeroelastic problem solved by Ventus2D i.e. solid body suspended in a fluid stream: 1 – rectangular calculation domain, 2 – uniform fluid stream, 3 – initial position of a solid body suspended in the stream, 4 – the body in motion and interacting with the fluid

The main idea behind DVM simulation is a vortex cloud and its mechanics executed in accordance with Eq. 6 and Eq. 7. In a general 3D case, the vortex cloud is a set of vorticity filaments that are, on the grounds of Helmholtz’s laws, closed or start and end on a solid body surface. For the case of 2D flows, all the filaments are straight lines perpendicular to the plane of analysis, therefore, they are illustrated as points on following figures and are just called discrete vortexes. The solid body immersed in the stream is covered with panels (Fig. 8). The panels are able to generate discrete vortexes on them. Each vortex induces



a velocity field according to the Biot-Savart law. The vorticity layer on the solid body is needed to cancel the velocity field inside the body because there is no fluid flow inside the body. Subsequently, the discrete vortexes generated on the panels are shed into the stream. Consequently, the velocity field of the fluid flow changes (free vortexes in the stream generate their velocity field) and new discrete vortexes on the panels have to be generated to cancel the velocity field inside the body. Free discrete vortexes are drifted and diffused in the stream according to Eq. 6 and Eq. 7 respectively. The resultant velocity field is a superposition of the oncoming homogeneous stream with velocity  $u_{AIR}$  and turbulent field generated by all discrete vortexes. The simulation job is a repetition of generating, shedding and propagating discrete vortexes in the stream. The structure of turbulence and macroscopic phenomena like resultant aerodynamic forces are the results of a direct simulation. The fundamental outcomes of the Ventus2D program are values and positions of discrete vortexes at every step of the computer simulation. Subsequently, the data enables finding velocity and pressure fields of the flow and calculates resultant aerodynamic forces acting on the solid body according to Eq. 8.

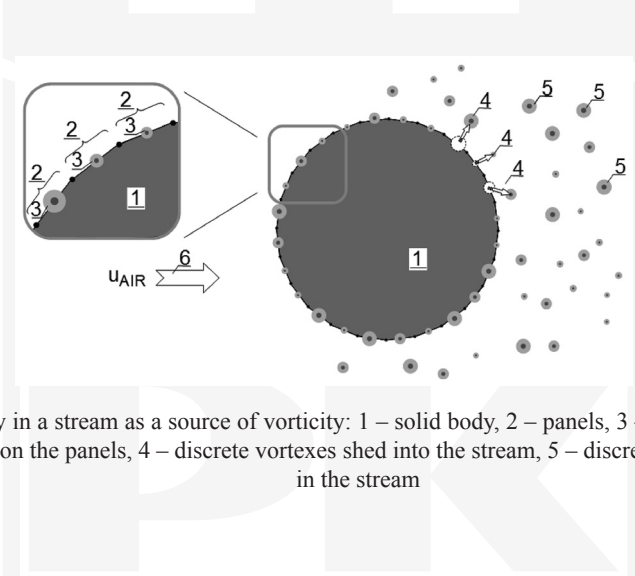


Fig. 8. Solid body in a stream as a source of vorticity: 1 – solid body, 2 – panels, 3 – discrete vortexes generated on the panels, 4 – discrete vortexes shed into the stream, 5 – discrete vortexes drifted in the stream

#### 4. The influence of surface roughness on the cross-flow around a circular cylinder (Review of literature)

The influence of surface roughness on the cross-flow around a circular cylinder has long been the subject of intense attention both from academic and practical points of view. Achnebach [6] described a wind tunnel experiment carried out in a range of Reynolds number  $1 \cdot 10^5 < Re < 3 \cdot 10^6$ . The object of the study was a cylinder with a diameter of 0.15 m. The levels of roughness examined were  $k_s/D = 0, 110 \cdot 10^{-5}, 450 \cdot 10^{-5}$  and  $900 \cdot 10^{-5}$  according to original notation, which gives  $f_1 = 0\%, 0.11\%, 0.45\%$  and  $0.90\%$ . Results clearly showed that a small degree of surface roughness did not change the course of the phenomena. There were still four characteristic regimes: subcritical, critical, supercritical and transcritical. Small surface roughness, e.g.  $f_1 < 1\%$ , seems to have no effect on aerodynamic drag force coefficient in the subcritical level but increases the coefficient in the supercritical level. However, the

values reported did not exceeded 1.3. Taking into consideration the critical and supercritical ranges, it was depicted that surface roughness changes the critical Reynolds number where the minimum of the coefficients is achieved. The minimum value still depends on the level of roughness and grows with increasing roughness and the values are equal to 0.4, 0.5, 0.72 and 0.72 respectively for the different levels of roughness.

Similar results are presented by Nakamura and Tomonari [7]. The range of Reynolds numbers covered here was  $4.0 \cdot 10^4 < Re < 1.7 \cdot 10^6$ . The diameter of the cylinder used in the experiment was 0.62m and the levels of surface roughness were  $r/D = 0, 6.5 \cdot 10^{-5}, 9.4 \cdot 10^{-5}, 18.5 \cdot 10^{-5}, 90 \cdot 10^{-5}, 226 \cdot 10^{-5}, 516 \cdot 10^{-5}$  and  $1000 \cdot 10^{-5}$  according to original notation or recalculated to  $f_1 = 0\%, 0.007\%, 0.009\%, 0.019\%, 0.09\%, 0.226\%, 0.516\%$  and  $1\%$  respectively. The experiment did not cover the subcritical regime. In the transcritical regime, the roughness again lost importance on the value of the drag force. The reported coefficient took the value of approximately 1. Transition from the critical to supercritical regime depends on the level of roughness, but the differences mainly concerned the critical Reynolds number and the minimum values were similar.

[8] considered bridge cables with a pattern-intended surface with a diameter of 140mm. The relative surface roughness defined by the depth of the indentations was 1%. The experiment intended to find aerodynamic forces carried out for the Reynolds number from  $0.3 \cdot 10^5$  to  $2.7 \cdot 10^5$ . The cable exhibited a very early transition into the supercritical region due to the level of surface roughness. The early flow transition agreed well with what was observed for circular cylinders with uniform roughness. The drag force coefficient at the lowest Re number was equal to 1.2 and decreased with increases to the number. Finally, it reached a value of 0.6 for  $Re > 1 \cdot 10^5$ .

## 5. Own research

All computer simulations were carried out in the same way. They were performed in a calculation domain with a size of  $2 \text{ m} \times 10 \text{ m}$  divided into  $10 \times 50 = 500$  cells (Fig. 9) used only as containers for free vortex particles. A cylinder with a 0.2 m in diameter and graded surface roughness (Fig. 2) was placed on the horizontal axis of symmetry at a distance of 1m from its start. This distance is sufficient for the boundary layer to form and propagate into the stream, which can be seen in Figs 10–14. The width of the domain was able to house the von Karman vortex street. Most of the discrete vortexes left the domain through the rear (right) side. In the computer simulations, the air stream has started abruptly from 0 do  $u_{\text{AIR}}$  (Fig. 15). For this reason, the first second of the outcome was rejected as being not real. After the first second, the process stabilised and the results could be used for macroscopic estimations. Every simulation consisted of 500 computational steps of constant length of  $\Delta t = 0.005 \text{ s}$ , which gave 2.5 s of the total process but only the last 1.5 s were valuable. However, the period of time of 1.5 s was long enough to determine the aerodynamic drag and extending it would only result in extra hours of computer work. The cross-section of the cylinder under study was covered with DVM panels numbering from 109 to 253 depending of the level of roughness with length  $\Delta L$  from 0.0045 m to 0.0058 m (see Table 2). The simulations were designed in order to keep the dimensionless parameter of the simulation step:

$$S = \frac{\Delta t \cdot u_{\text{AIR}}}{\Delta L} \quad (9)$$

in the range of 1 to 25.

The oncoming fluid stream was dry air with a uniform value in the calculation domain (Fig. 9). The velocity of the stream  $u_{\text{AIR}}$  took values of 5 m/s, 10 m/s, 15 m/s, 20 m/s, which gave Reynolds number values of  $0.7 \cdot 10^5$ ,  $1.3 \cdot 10^5$ ,  $2.0 \cdot 10^5$ ,  $2.7 \cdot 10^5$  respectively at a kinematic viscosity of  $1.5 \cdot 10^{-5} \text{ m}^2/\text{s}$ . Finally, 20 computer simulations were carried out, which took about 72 hours of computational time on 32-bit PC computer with CPU  $2 \times 2.10 \text{ GHz}$  and 2 GB RAM.

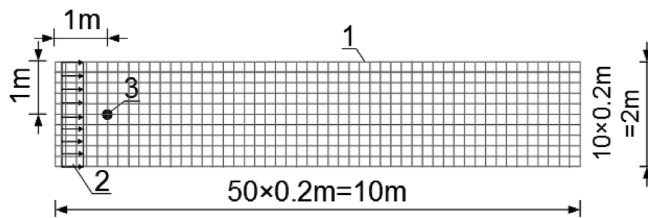


Fig. 9. The cylinder under study in a calculation domain: 1 – calculation domain divided in 500 square cells, 2 – uniform fluid stream, 3 – stationary cylinder

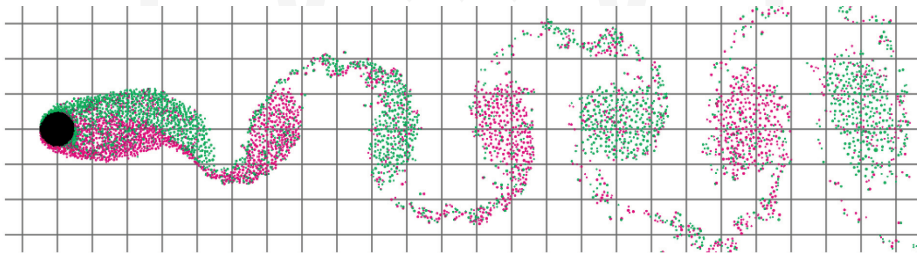


Fig. 10. Snapshot of DVM simulation for  $u_{\text{AIR}}=10 \text{ m/s}$ , roughness level: a (Fig. 2), simulation step 500

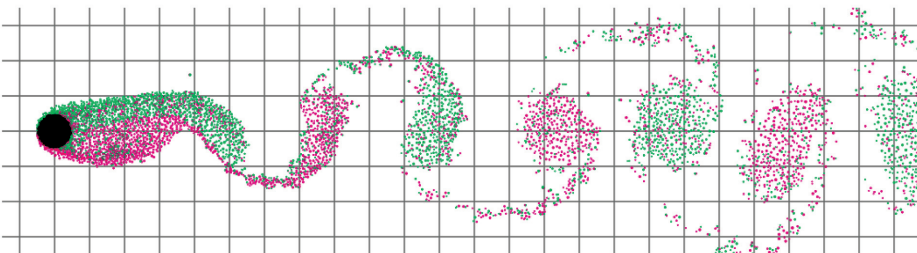


Fig. 11. Snapshot of DVM simulation for  $u_{\text{AIR}}=10 \text{ m/s}$ , roughness level: b (Fig. 2), simulation step 500

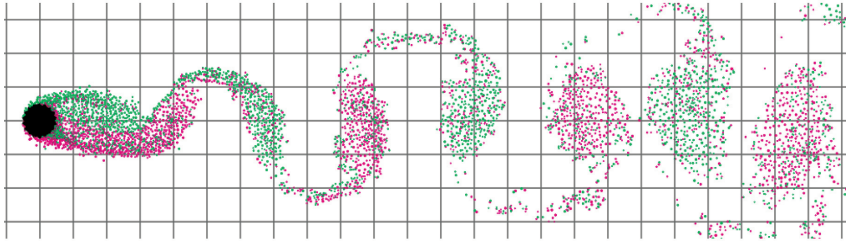


Fig. 12. Snapshot of DVM simulation for  $u_{\text{AIR}}=10$  m/s, roughness level: c (Fig. 2), simulation step 500

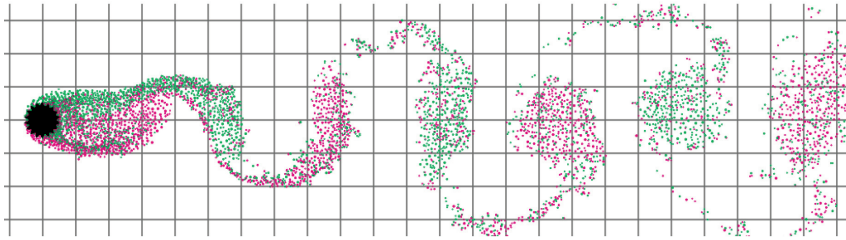


Fig. 13. Snapshot of DVM simulation for  $u_{\text{AIR}}=10$  m/s, roughness level: d (Fig. 2), simulation step 500

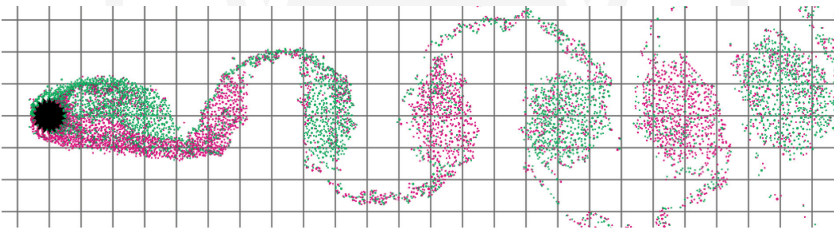


Fig. 14. Snapshot of DVM simulation for  $u_{\text{AIR}}=10$  m/s, roughness level: e (Fig. 2), simulation step 500

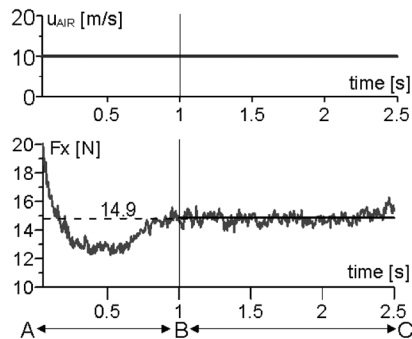







Fig. 15. Stabilization of the calculation process for abruptly started stream velocity  $u_{\text{AIR}}$  (a) by the example of aerodynamic drag force  $F_x$  (b). The range A-B was rejected and the mean aerodynamic force was calculated in the range B-C. Diagram for case:  $u_{\text{AIR}}=10$  m/s, roughness level: d acc. to Fig. 2

**Comparison of DVM models and the dimensionless parameter of a simulation step**

Level of roughness	DVM panels		$S = \Delta t u_{\text{AIR}} / \Delta L$
	Total numbers	Length $\Delta L$ [m]	
a) 	109	0.0058	4.3 ÷ 17.2
b) 	145	0.0045	5.5 ÷ 22.1
c) 	145	0.0050	5.0 ÷ 19.9
d) 	181	0.0053	4.7 ÷ 18.9
e) 	253	0.0049	5.1 ÷ 20.2

## 6. Results

The output of computer simulations was the records of 20 air flows around the cylinder. Each record consists of 500 snapshots. Every snapshot is a trace of the discrete vorticity field, sample of which are presented on figures from 10 to 14, where the colour green indicates vortices of a clockwise circulation. Positions and values of discrete vortices enable finding the velocity and pressure field of the flow and finally, finding the resultant aerodynamic forces such as aerodynamic drag. The values and dimensionless coefficients corresponding to them are presented in Table 3. The drag coefficient has been calculated using formula:

$$C_X = \frac{F_X}{q \cdot D_{\text{MEAN}}} \quad (10)$$

where  $F_X$  is a drag force for a unit length of the cylinder [N/m],  $q = 1/2 \cdot 1.21 \text{ kg/m}^3 \cdot u_{\text{AIR}}^2$  is stream pressure and is equal to 15.1 Pa, 60.5 Pa, 136.1 Pa, 242.0 Pa for  $u_{\text{AIR}} = 5 \text{ m/s}$ , 10 m/s, 15 m/s, 20 m/s respectively,  $D_{\text{MEAN}}$  – mean diameter of the cylinder. Using a mean diameter instead of a closing diameter is justified by the method by which the surface roughness is treated. The roughness is not a change in shape but perturbation of the original surface. The shape and dimensions of the original surface do not change. This is a very convenient approach to the problem from an engineering point of view.

The change in the coefficient against increasing roughness is depicted on figures from 20 to 22. At this point, the starting value of  $C_X$  which is less than 1.2, needs a note. DVM computer simulations do not cover the whole spectrum of solid–fluid interaction. Such simulations neglect i.a. turbulence of oncoming air stream, effects of the 3D nature of the flow, impact of surrounding walls and of course the results incorporate many other physical simplifications. Finally, the values obtained from DVM 2D computer simulations are usually lower than experimental results [3, 5].

**Aerodynamic drag force  $F_x$  [N/m] acting on the cylinder and corresponding drag coefficient  $C_x$  [-] corresponding to air stream velocity  $u_{AIR}$  [m/s] for five different levels of surface roughness**

	$u_{AIR} = 5; Re = 0.7 \cdot 10^5$			$u_{AIR} = 10; Re = 1.3 \cdot 10^5$			$u_{AIR} = 15; Re = 2.0 \cdot 10^5$			$u_{AIR} = 20; Re = 2.7 \cdot 10^5$		
	$F_x$	$C_x$		$F_x$	$C_x$		$F_x$	$C_x$		$F_x$	$C_x$	
a)	3.31	1.09	100%	12.89	1.07	100%	29.31	1.08	100%	52.00	1.07	100%
b)	3.36	1.11	102%	13.03	1.08	105%	29.10	1.07	99%	51.82	1.07	100%
c)	3.60	1.19	109%	13.94	1.15	112%	30.02	1.10	102%	51.90	1.07	100%
d)	4.47	1.48	135%	14.88	1.23	120%	33.28	1.22	114%	59.66	1.23	115%
e)	4.67	1.54	141%	18.04	1.49	145%	39.73	1.46	136%	74.28	1.53	143%

Looking at the columns in Table 3, we can state that increases in roughness result in increases in aerodynamic force and its coefficient for the same air stream velocity. This is in line with intuition and is therefore unsurprising. Owing to the critical regime of the flow, one should expect a decrease in the aerodynamic force caused by the increase of stream velocity for a given level of surface roughness. Comparing values in rows in Table 3, we can observe the effect for the levels of roughness indicated by 'b', 'c', and 'd'. For the level marked by 'e', the value first decreases and then grows. For the first level named 'a', the effect does not occur and the value does not change much. The last column in Table 3 shows that at higher air stream speed, the modest roughness of surface does not affect the aerodynamic drag.

The resulting drag force is related to a turbulent boundary layer which is formed by the surface of the solid body. Undoubtedly, roughness of the surface affects the layer. Figures from 16 to 19 depict boundary layers developed in DVM computer simulations. It can be easily discovered that the boundary layer stays similar for the 3 first levels of surface roughness, i.e. 'a', 'b', 'c', and is apparently different for the last level (e). The last boundary layer is thicker and does not cover the body with a uniform film. The level marked by d may be considered as a transition stage. This observation corresponds with diagrams of  $C_x$  presented in figures 20, 21 and 22. The last value of the coefficient differs significantly from the first three, which have similar values.

Taking into account all the observations, it is possible to state that small surface roughness is covered with a turbulent boundary layer and does not change the aerodynamic drag much. One can say that the roughness is hidden in the layer. Table 3 and diagrams of  $C_x$  (Figs 20, 21, 22) clearly show that the influence of the roughness strongly depends on the air stream. For  $u_{AIR} = 15$  m/s and 20 m/s, the roughness of level 'c' is still small but it is significant at  $u_{AIR} = 5$  and 10 m/s. This can be explained by the fact that along with increasing stream velocity, the importance of viscous forces decreases. In other words, the Reynolds number grows. Therefore, the limit level of roughness, below which the roughness can be omitted, should be related to the Reynolds number. Such an approach seems to be appropriate but is of little use for objects that have to stay to wind of broad spectrum of speed. Taking into consideration the last, the limit must be set up to be safe in all cases. Assuming that a 5% error is acceptable in engineering estimations of aerodynamic drag force, the two first levels

of roughness can be neglected. Using the parameters of roughness introduced earlier, the rule may be expressed quantitatively. The surface roughness can be neglected in engineering estimations of  $C_x$  if  $f_1 < 3\%$ ,  $f_2 < 5\%$ ,  $f_3 < 4\%$ . The values have been rounded to the nearest whole numbers.

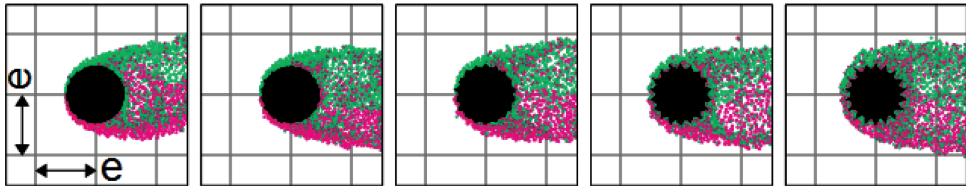


Fig. 16. Visualisation of discrete boundary layer formed at an air stream velocity of  $u_{\text{AIR}} = 5$  m/s for all the levels of roughness from a to e. Reference dimension  $e = 0.2$  m

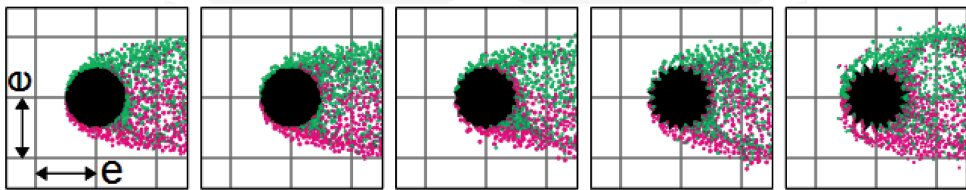


Fig. 17. Visualisation of discrete boundary layer formed at an air stream velocity of  $u_{\text{AIR}} = 10$  m/s for all the levels of roughness from a to e. Reference dimension  $e = 0.2$  m

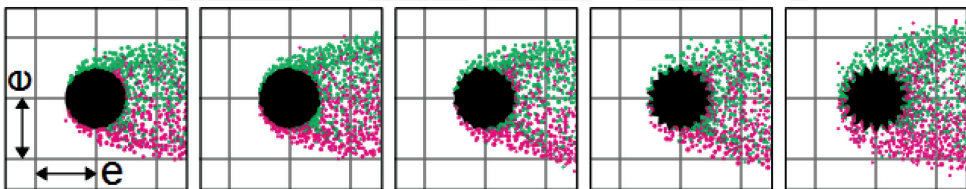


Fig. 18. Visualisation of discrete boundary layer formed at an air stream velocity of  $u_{\text{AIR}} = 15$  m/s for all the levels of roughness from a to e. Reference dimension  $e = 0.2$  m

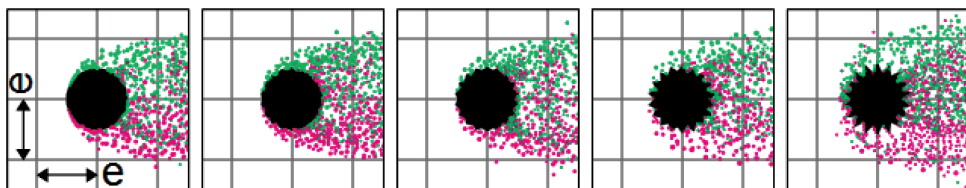


Fig. 19. Visualisation of discrete boundary layer formed at an air stream velocity of  $u_{\text{AIR}} = 20$  m/s for all the levels of roughness from a to e. Reference dimension  $e = 0.2$  m

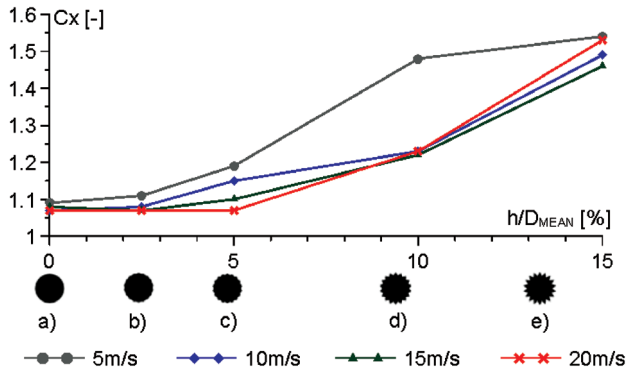


Fig. 20. Diagram of aerodynamic drag coefficient  $C_x$  against growing surface roughness described by parameter  $f_1 = h/D_{MEAN}$  for different air stream velocity

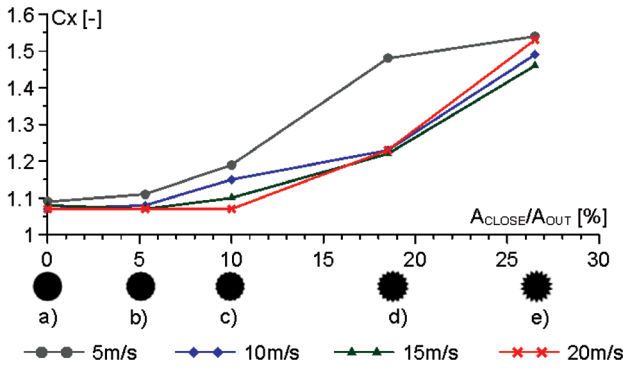


Fig. 21. Diagram of aerodynamic drag coefficient  $C_x$  against growing surface roughness described by parameter  $f_2 = A_{CLOSE}/D_{OUT}$  for different air stream velocity

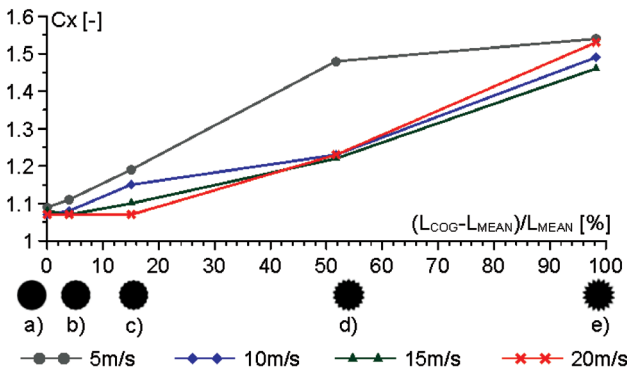


Fig. 22. Diagram of aerodynamic drag coefficient  $C_x$  against growing surface roughness described by parameter  $f_1 = (L_{COG}-L_{MEAN})/L_{MEAN}$  for different air stream velocity



Another question was regarding when the level of roughness should be treated as a change in the original shape. The criterion here can be changed in the structure of boundary layer. Any perturbation in the smooth surface can be treated as roughness for as long as the form of the boundary layer remains the same. Figures from 16 to 19 show that the three first levels of roughness (i.e. 'a', 'b', and 'c') generate a very similar boundary layer form but the last one (f) varies considerably. The next to the last case (d) seems to be the transitional stage and can be treated as the roughness limit. Using the parameters of roughness, the limit should be set to  $f_1 < 10\%$   $f_2 < 20\%$   $f_3 < 50\%$ . The values have been rounded to the nearest ten due to estimation that is not precise.

Finally, there is the possibility to determine the range of surface perturbation that cannot be neglected and that is still regarded as roughness of the original shape and not a change in shape. Using the parameters, the range is:  $3\% < f_1 < 10\%$ ,  $5\% < f_2 < 20\%$ ,  $4\% < f_3 < 50\%$ . In the range, the influence of surface roughness is significant and should be counted while estimating aerodynamic drag. The data collected in the research is, alas, not adequate to find such correction factors. The factors seem to be related to the wind speed or the Reynolds number and will be the subject of further research. The parameter of surface roughness also may be significant. The parameters  $f_3$  vs.  $f_1$  and  $f_2$  narrow the range of negligible surface roughness and stretch the range of significant roughness (see Figs 20, 21 and 22).

## 7. Conclusions

Computer simulations of air flow around a cylinder with a surface with a high level of roughness were carried out in order to find the relationship between surface roughness and drag coefficient. The analyses were limited to the critical region of the flow. The critical region arose due to the Reynolds number range covered in the simulations and the roughness that generated the turbulent boundary layer. Despite the high level of roughness, the phenomena proceeded as expected for a smooth cylinder. Since in many engineering estimations of aerodynamic drag force coefficient only the upper limits are important, it was possible to assess the level of roughness at which the roughness became important and the limit when the roughness should be treated as a change in shape.

## References

- [1] Lewis R.I., *Vortex element methods for fluid dynamic analysis of engineering systems*, Cambridge University Press, 2005.
- [2] Turkiyyah G., Reed D., Yang J., *Fast vortex methods for predicting wind – induced pressures on buildings*, Journal of Wind Engineering and Industrial Aerodynamics, Vol. 58, 1995.
- [3] Taylor I., Vezza M., *Predition of unsteady flow around square and rectangular section cylinder using a discrete vortex method*, Journal of Wind Engineering and Industrial Aerodynamics, Vol. 82, 1999, 247-269.

- [4] Larsen A., Walther J.H., *Aeroelastic analysis of bridge girder sections based on discrete vortex simulation*, Journal of Wind Engineering and Industrial Aerodynamics, Vol. 67-68, 1997.
- [5] Nowicki T., *Influence of boundary condition implementation in discrete vortex method on aeroelastic response of bridge decks*, Monografie – Politechnika Lubelska, Lublin 2012 (in Polish).
- [6] Achnebach E., *Influence of surface roughness on the cross-flow around a circular cylinder*, Journal of Fluid Mechanics, Vol. 46(2), 1970, 321-335.
- [7] Nakamura Y., Tomonari Y., *The effects of surface roughness on the flow past circular cylinder at high Reynolds numbers*, Journal of Fluid Mechanics, Vol. 123, 1981, 363-378.
- [8] Kleissl K., Georgakis C.T., *Comparison of the aerodynamics of bridge cables with helical fillets and a pattern-indented surface*, Journal of Wind Engineering and Industrial Aerodynamics, Vol. 104-106, 2012, 166-175.

